Electronic Supplementary information

Nanomechanical Elasticity and Fracture Studies of Lithium Phosphate (LPO) and Lithium Tantalate (LTO) Solid-state Electrolytes

Maedeh Amirmaleki,[a] Changhong Cao,[a] Biqiong Wang,[b] Yang Zhao,[b] Teng Cui,[a] Jason Tam,[c] Xueliang Sun,[*b] Yu Sun[a] and Tobin Filleter[*a]

[a]Department of Mechanical and Industrial Engineering, University of Toronto, 5 King's College Road, Toronto, ON, Canada, M5S 3G8. E-mail: filleter@mie.utoronot.ca
[b]Department of Mechanical and Materials Engineering, University of Western Ontario, London, Ontario, Canada N6A 5B9. E-mail: xsun9@uwo.ca
[c]Department of Materials Science and Engineering, University of Toronto, 184 College St, Toronto, ON, Canada, M5S 3E4

1. Selected area diffraction pattern (SADP) of LTO thin film

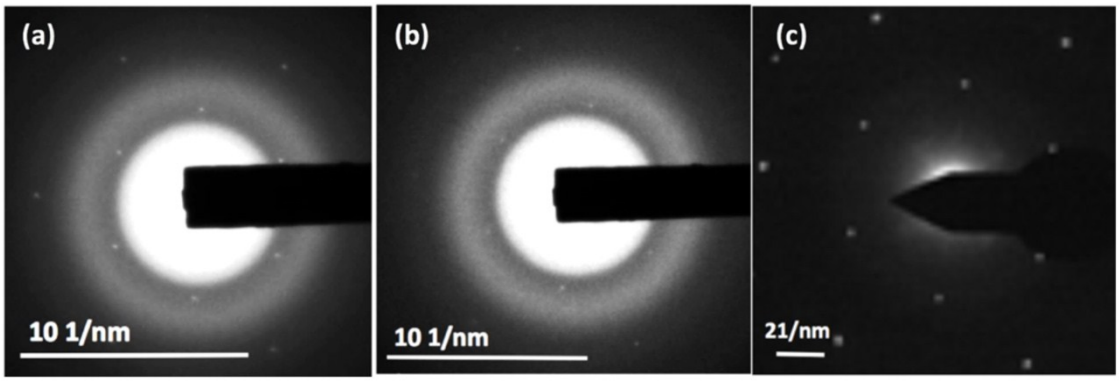

Figure S1 SADP of a) LTO 25 nm, b) LTO 15 nm, and c) single layer CVD graphene from Ted Pella Inc.[1], white dots in all images are indication single layer graphene pattern.

SADP of LTO 15 nm and 25 nm was obtained with Hitachi HF-3300 scanning transmission electron microscopy (STEM). The SSE thin films are containing amorphous layer of Al_2O_3 (around 2nm), single layer graphene, and amorphous LTO 15 nm (as in Figure S1a) and 25 nm (as in Figure S1b). The halo in Figure S1 a and b proves the amorphous structure of the Al_2O_3 and LTO layers. The white dots in the SADPs belong to single layer graphene which follows the same pattern of CVD single layer graphene from supplier as shown in Figure 1Sc.

2. Scanning electron microscopy (SEM) images and Electron Energy-Dispersive X-ray (EDS) Elemental Mapping of SSE thin films

SEM and EDS were preformed using Hitachi HF-3300 STEM at 300 kV. The EDS elemental mapping was used to investigate the nature of the circular particles over the SSE as shown with red arrows in the Figure S2. The EDS mapping revealed that the circular particles are containing the same elements as the SSEs films, and no other elemental peak was observed for the particle shape areas.

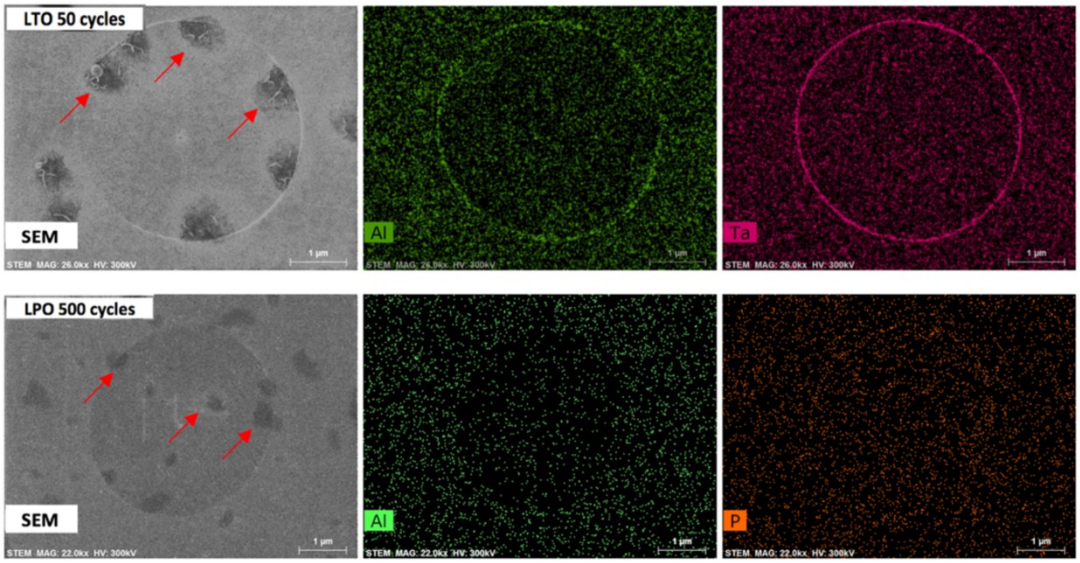

Figure S2 SEM images and EDS elemental maps of intact LTO (top) and LPO (bottom) thin films.

3. Data Processing

In order to obtain the force-film deflection curves, it is first needed to define the point that both force and film deflection is zero. Figure S3 shows the raw force data from a force-film deflection of a LPO free-standing film. During loading, first, the AFM tip deflects downward to the film (point A – known as a "jump into contact") as a result of van der Walls attraction and then deflects upward as the tip pushes against the film. The force-film deflection exhibits a linear behavior after point A, and the curve reaches a zero force value (point B). Point B is considered as the zero force point, and the zero deflection point meaning that the cantilever becomes straight, and the film is not under any deflection force. The obtained zero points are used as the initial point of the force-film deflection curves shown in the manuscript. While alternative techniques to find the zero points are available in the literature[2], we have used a simplified method to find the zero point for the force-film deflection curves as it is not appropriate to fit an isotropic film model to the elastic curves to obtain the modulus due to the complexity of the multilayered materials systems studied herein. This technique was used to find zero points for all of the films at all thicknesses. For all of the measurements film deflection is obtained by subtracting the tip deflection from the z piezo displacement: $\delta_{film} = \delta_{piezo} - \delta_{cantiliver}$. Raw data of force, piezo displacement and cantilever deflection are collected during loading and unloading.

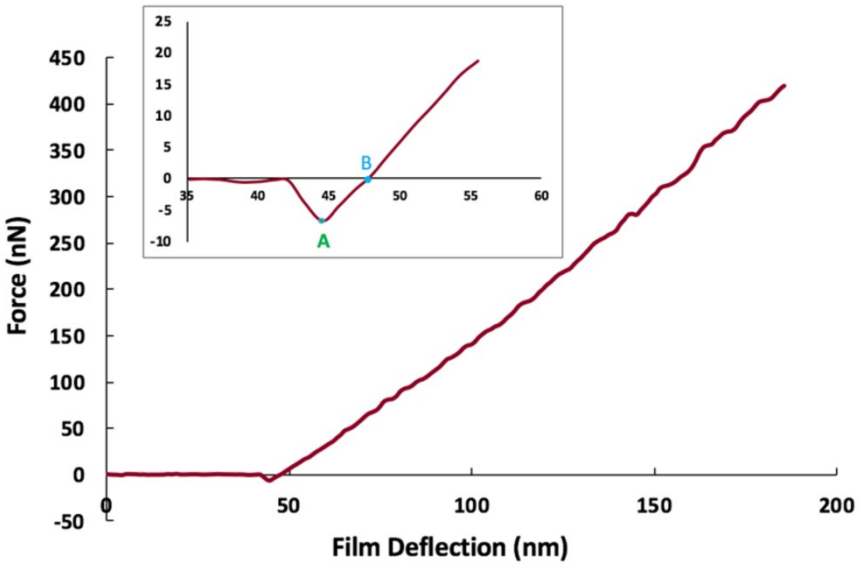

Figure S3 Measured force vs. film deflection for LPO 6 nm films. The inset shows the close look of the zero force point.

4. Representative elastic loading-unloading force curve vs film deflection

A representative loading-unloading curve vs film deflection of the SSE thin films using Asylum MFP-3D atomic force microscope (AFM) reveals no significant hysteresis between loading-unloading curves (Figure S4). This indicates that bonding between layers in thin structured films, and between the graphene/substrate was strong enough to avoid any significant slippage between layers.

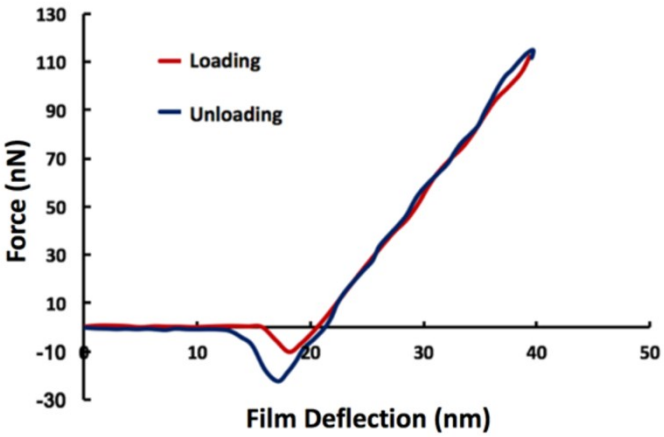

Figure S4 An example of loading-unloading force vs film deflection in elastic region with no hysteresis.

5. Elastic force vs film deflection curve of SSE thin film

Figure S5 shows an example of AFM force-film deflection curve of four samples from very thin SSE film (LTO 5 nm and LPO 6nm) loaded to maximum normal force of 100 nN at a constant displacement rate of 10 μms^{-1}. Similar to the examples presented in Figure 2b, the results of elastic deflection of all samples of SSE thin films were consistent and repeatable.

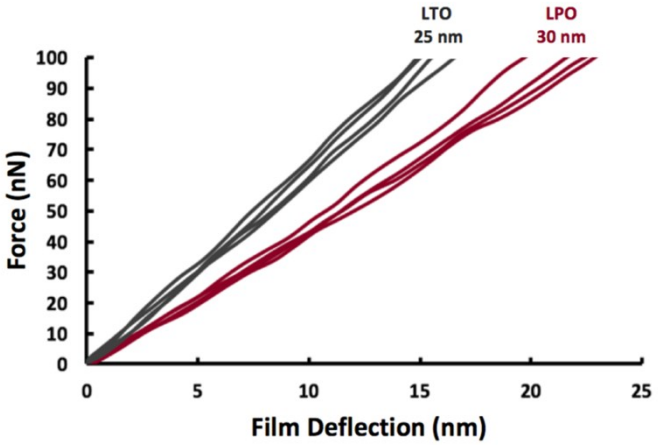

Figure S5 Elastic force-film deflection curve from deflection of four samples of LTO (25 nm) and LPO (30 nm) thin films showing repeatability and consistency.

6. Modeling of elastic behavior

Equation 1 shows a model that was used to calculate the elastic modulus of suspended circular 2D films under a central load which is a combination for linear and nonlinear mechanical response of the ultra-thin films.[2–7]

$$F = \left[\frac{4\pi E}{3(1-\nu^2)} \cdot \left(\frac{t^3}{R^2}\right)\right]\delta + (\pi T)\delta + \left(\frac{q^3 ET}{R^2}\right)\delta^3 \qquad \text{Eq. 1}$$

where E and ν are the Young's modulus and the Poisson ratio, t is the thickness of the nanosheet, R is its radius, T its pre-tension and $q = 1/(1.05 - 0.15\nu - 0.16\nu^2)$.

The first term in Eq. 1 corresponds to the mechanical behavior of a plate (bending dominated, linear term) with specific bending rigidity. The second term is pretention in the stretched membrane, and the third term corresponds to mechanical response (bending stiffness) of a stretch dominated membrane (non-linear term). By increasing the film thickness bending rigidity increases by a cubic dependency (t^3) and plate behavior dominates. The force-deflection curves of all LPO and LTO films were linear at all thicknesses. Therefore, all the samples behave as plates and the slope of the force-deflection curve indicates the bending rigidity of the films. The slope values of the force-deflection curves of all LPO and LTO films as well as 5 nm Al_2O_3 films are presented in Table 1. The slope values for LTO films are higher than LPO films at all thicknesses which shows higher stiffness for LTO films as compared to LPO films. The slope value of 5nm ALD Al_2O_3 over graphene is similar to that of 5nm LTO and 6nm LPO which can emphasize the dominant effect of the Al_2O_3 capping layer and graphene support layer on the very thin SSE films. Since the intrinsic mechanical properties such as elastic modulus of the Al_2O_3 capping layer and LPO and LTO films at the nanometer scale are unknown, calculating E of the structures using this model is not practical. However, the general trend of higher stiffness of LTO as compared to LPO films is clearly evident from the experimental data.

Table 1. Comparing the slope of force-deflection curves

Thin film sample		Stiffness
LTO (Graphene/LTO/Al_2O_3)	**5 nm LTO** (7.33 nm G/LTO/Al_2O_3)	**2.91+/-0.02 N/m**
	15 nm LTO (17.33 nm G/LTO/Al_2O_3)	**4.33+/- 0.32 N/m**
	25 nm LTO (27.33 nm G/LTO/Al2O3)	**6.74+/- 0.19 N/m**
LPO (Graphene/LPO/Al_2O_3)	**6 nm LPO** (8.33 nm G/LPO/Al_2O_3)	**2.66+/- 0.01 N/m**
	18 nm LPO (20.33 nm G/LPO/Al_2O_3)	**3.43+/- 0.03 N/m**
	30 nm LPO (32.33 nm G/LPO/Al_2O_3)	**5.58+/- 0.05 N/m**
Al_2O_3 (Graphene /Al_2O_3)	**5 nm Al2O3** (5.33 nm G/Al_2O_3)	**2.8+/- 0.04 N/m**

7. Aluminum Element mapping on fractured SSE films

The LPO and LTO films were coated with thin ALD Al_2O_3 (~2 nm) which is an excellent coating material to address interfacial issues.[8] No hysterias in force-film deflection curve was observed for the LPO and LTO film that suggested strong adhesion between the coating layer Al_2O_3 and LOP and LTO films in the elastic regime. Delamination occurred at a very high range of forces. LPO films show more severe delamination as a results of interlayer damages and plastic deformation of LPO before fracture. However, TEM imaging did not show any evidence of delamination in the interface of Al_2O_3 and LPO and LTO films (shown in Figure S6). Accordingly bonding between the layers is considered as nearly perfect bonding even under huge forces that led to fracture and deformation of the films.

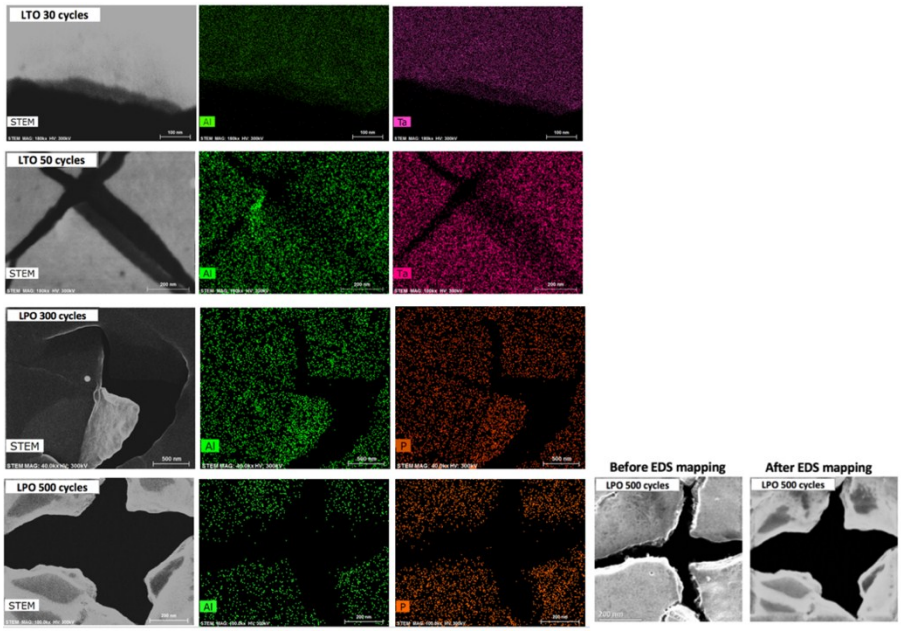

Figure S6 STEM images and EDS elemental map of the fractured LTO and LPO thin films. The Al elemental mapping show that the fractured and delaminated films were containing Al and no detachment in the interface of Al_2O_3 and LPO or LTO film was visible. Bottom right image shows that the LPO 500 cycles affected by the beam and deformed severely during EDS signal collection.

8. Hysteresis in force-deflection curves at high range of forces

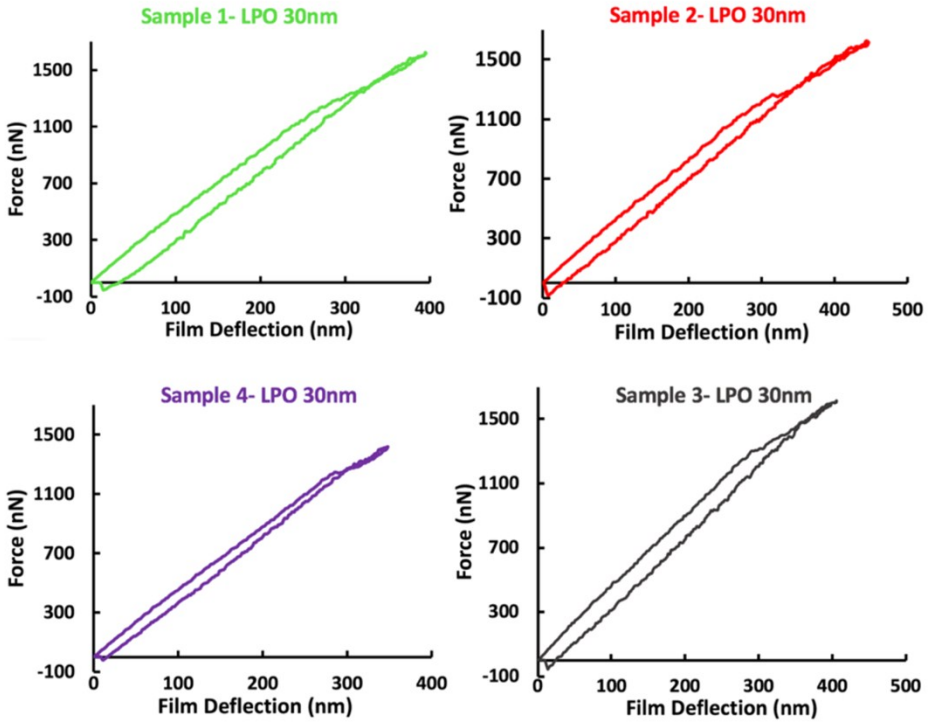

Figure S7 Visible hysteresis in force-film deflection curves of LPO 30 nm films. The hysteresis was observed for all samples loaded to a similar range of forces (1300 nN-1700 nN).

Hysteresis in the loading/unloading curves was observed in force-film deflection curves of LPO films at high range of forces (1300 nN to 1700 nN) which indicates energy dissipation prior to the onset of failure. Figure S7 shows examples of the repeatability of the hysteresis in force-film deflection curves for 30 nm LPO films.

9. AFM diamond tip diameter measurement before and after tests

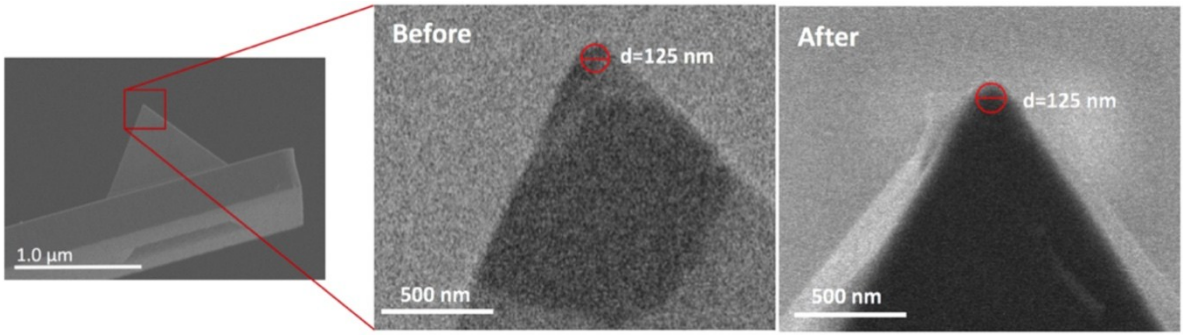

Figure S8 SEM images of the diamond tip was used for AFM deflection before and after tests on thin films.

The AFM diamond tip was imaged using SEM before and after the deflection (shown in Figure S8) tests to ensure that no damage was occur during testing. Also, the diameter of the tip did not change before and after AFM deflection tests of the SSE thin films.

References

1 https://www.tedpella.com/Support_Films_html/Graphene-TEM-Support-Film.htm.

2 C. Lee, X. Wei, J. W. Kysar and J. Hone, *Science (80-.).*, 2008, **321**, 385–389.

3 J. H. Woo, J. E. Trevey, A. S. Cavanagh, Y. S. Choi, S. C. Kim, S. M. George, K. H. Oh and S.-H. Lee, *J. Electrochem. Soc.*, 2012, **159**, A1120–A1124.

4 S. Timoshenko, *Theory of Plates and Shells*, McGraw-Hill, London, 1940.

5 A. Castellanos-Gomez, M. Poot, A. Amor-Amorós, G. A. Steele, H. S. J. van der Zant, N. Agraït and G. Rubio-Bollinger, *Nano Res.*, 2012, **5**, 550–557.

6 K. Liu, Q. Yan, M. Chen, W. Fan, Y. Sun, J. Suh, D. Fu, S. Lee, J. Zhou, S. Tongay, J. Ji, B. Neaton and J. Wu, *Nano Lett.*, 2014, **14**, 5097–5103.

7 R. Zhang, V. Koutsos, R. Cheung, R. Zhang, V. Koutsos and R. Cheung, *Appl. Phys. Lett.*, 2016, **108**, 042104.

8 Y. Zhao, K. Zheng and X. Sun, *Joule*, 2018, **2**, 2583–2604.